Chapter 16
Application of Nonlocal Fick's Law Within Micropolar Approach

Ksenia Frolova, Nikolay Bessonov, and Elena Vilchevskaya

Abstract The paper is concerned with modeling of stress-induced diffusion within the framework of the micropolar approach. The specificity of the model accounting for stress-strain state of the host material by means of additional thermodynamic driving force in the form of gradient of chemical potential is discussed. The considered model represents a generalization of the known corresponding model developed within the framework of the classical approach. The proposed generalization allows one to account for size effects while modeling the diffusion process. The main focus is on modeling of the skin effect manifested near the perturbation surface. It is shown that accounting for couple stress interactions between material particles results in a significant excess of diffusing impurity in the vicinity of the border. An axially symmetric problem is solved and investigated in detail. Various types of boundary condition on the outer border are used to demonstrate the general specificity of the developed model. Qualitative and quantitative effect of non-classical material parameters is discussed.

Key words: Stress-induced diffusion · Chemical potential · Micropolar continua · Size effect · Skin effect

16.1 Introduction

The paper models stress-induced diffusion within the framework of the micropolar approach to account for size effects. Problem of diffusion in solids has applications in various fields of science such as geology, metallurgical engineering, etc. The accumulation of harmful impurities in metals can worsen material properties and

Ksenia Frolova · Nikolay Bessonov · Elena Vilchevskaya
Institute for Problems in Mechanical Engineering RAS, Bolshoy pr., 61, V.O., St. Petersburg, 199178, Russian Federation,
e-mail: fkp@ipme.ru, bnm@ipme.ru, ven@ipme.ru

H. Altenbach et al. (eds.), *Sixty Shades of Generalized Continua*,
Advanced Structured Materials 170, https://doi.org/10.1007/978-3-031-26186-2_16

even lead to its damage. In particular, a widespread problem of material science is hydrogen embrittlement of metal alloys [1, 2]. It is known that mechanical loading, as well as the presence of inhomogeneities of different nature can affect mass transport process in a host material. In particular, a local increase of impurity can take place [3]-[5]. The question arises of accounting for the influence of stress-strain state and microstructure of solid on diffusion of impurity.

The diffusion process depends on both the diffusion characteristics of impurity itself and on the state of the host material lattice. In general, diffusion can be modeled from the standpoint of rational mechanics or within the framework of thermodynamics. In the first case modeling of the diffusion process is based on the principles of continuum mechanics which is implementation of conversation laws for multi-component media supplemented by appropriate constitutive equations [6, 7]. The diffusion flux can be expressed in terms of the velocity of impurity. It depends on various fields, in particular, on the concentration gradient, as well as stresses and strains in the host material. The solution of the corresponding nonlinear kinematic equation is a challenging task, so simplifying assumptions on interaction between the impurity and the main structure are usually made [7]-[9]. Within a more widely used thermodynamic approach, the diffusion flux is expressed directly as a gradient of chemical potential. In the most simple case of the chemical potential of ideal gas, the constitutive equation for the diffusion flux reduces to the phenomenological Fick's first law relating the diffusion flux to the concentration gradient. Fick's law can be considered as a local one in that it relates the local flux to the local concentration gradient [10]. Li et al. [11] and Larche and Cahn [12, 13] considered a more complex expression for the chemical potential and accounted for the influence of the trace of the stress tensor caused by the eigenstrains due to accumulation of impurity. Larche and Cahn [12, 13] referred to the amended Fick's law as to nonlocal one, since the chemical potential is expressed in terms of the local stress, which depends on the solution of a boundary-value problem. Wu [10] studied the mutual influence of self-stresses and another forms of internal stresses and took chemical potential of the isotropic host material to be proportional to the trace of the Eshelby energy-momentum tensor introduced in [14] within classical elasticity.

So that, the introduction of the chemical potential of the system "impurity-solid host material" allows one to describe stress-induced diffusion. Obviously, such an approach can be extended to description of diffusion process in media modeled by microstructure-informed continua to account for size effects like the presence of inhomogeneities or skin effects. It is known that gradient theory accounts for the microstructure by means of accounting for deformation gradient in the expression for the elastic strain energy [15]-[18], micropolar theory accounts for traction at micro-scale by means of introduction couple stress interactions between material particles [19]-[21]. Such an accounting for internal degrees of freedom leads to necessity to introduce a more general expression for the Eshelby energy-momentum tensor, which depends on the stress-strain state of material. Within the frame of the present research we focus on modeling of stress-induced diffusion within micropolar approach. Expressions for the Eshelby tensors of non-linear and linear micropolar continua were obtained respectively in [22, 23]. In [24] we developed a micropolar

model of stress-induced diffusion accounting for the chemical potential in a form of the trace of the Eshelby energy-momentum tensor. The specificity of this model was investigated on the base of the boundary-value problem with Dirichlet condition on the outer border. The solution of the problem allowed to describe skin effect that is accumulation of impurity in the vicinity of the border. The present research discusses the specificity of the model in a broader sense and solves the problems with different types of the boundary condition to demonstrate that skin effect is caused by the presence of inhomogeneities in material, but not by specific conditions of saturation.

16.2 Diffusion in Media Modeled by Micropolar Continuum

The paper is concerned with modeling the diffusion process in a solid taking into account its microstructure influence. To this end, we generalize a known model of stress-induced diffusion usually used within the framework of the classical theory to describe mass transport process in a solid modeled by micropolar continuum. So that, the present research is multidisciplinary in that sense it makes an attempt to combine ideas of two theories to account for the influence of stress-strain state of the host material on diffusion process in the vicinity of some kind of perturbation area that is inhomogeneity, outer border, etc. The paper accounts for the influence of inner stresses and strains on diffusion process by means of chemical potential of host material as suggested in [10, 25]. The basic ideas of micropolar theory can be found in the reviews [19]-[21].

For simplicity we restrict ourselves to modeling diffusion in physically isotropic and geometrically linear solid host material. In the following we first provide the main formulas of diffusion problem and then the main formulas of micropolar elasticity.

The concentration of impurity c can be obtained from the mass balance that is

$$\frac{\mathrm{d}}{\mathrm{dt}} \int_V c \mathrm{dV} = - \int_{\mathrm{S}} \boldsymbol{n} \cdot \boldsymbol{J} \mathrm{dS}, \tag{16.1}$$

where d/dt is the total derivative with respect to time, $\boldsymbol{n}$ is the outer normal to surface S surrounding the elementary domain V, $\boldsymbol{J}$ is the diffusion flux.

The mass balance in local form reduces to

$$\frac{\mathrm{dc}}{\mathrm{dt}} = -\nabla \cdot \boldsymbol{J}. \tag{16.2}$$

In accordance with linear nonequilibrium thermodynamics, diffusion flux is related to the gradient of chemical potential μ of the system "impurity-host material" as

$$\boldsymbol{J} = -Mc\nabla\mu, \tag{16.3}$$

where M is the impurity mobility ($M = D/RT$, here D is the diffusion coefficient, R is the universal gas constant, T is the absolute temperature).

The chemical potential μ is a sum of the chemical potentials of the diffusing impurity and the host material. Equating the chemical potential of the impurity to the chemical potential of the ideal gas, one can rewrite Eq. (16.3) in the following form:

$$\boldsymbol{J} = -D\left(\nabla c + c\frac{1}{RT}\nabla\mu_S\right), \tag{16.4}$$

where μ_S represents the chemical potential of solid host material.

The first term in Eq. (16.4) represents the diffusion flux due to the concentration gradient, whereas the second term represent the diffusion flux due to the additional thermodynamic driving force $\boldsymbol{F} = \nabla\mu_S/RT$. The chemical potential of a solid is as follows [10]:

$$\mu_S = M_S\left(f_S^0 + \frac{1}{\rho_S}\mathrm{tr}\boldsymbol{\Sigma}\right), \tag{16.5}$$

where M_S is the molar mass of solid host material, f_S^0 is the free energy density of host material in a stress-free state, ρ_S is the density of host material, $\boldsymbol{\Sigma}$ is the Eshelby energy-momentum tensor, "tr" denotes trace of a second-order tensor. So, the additional thermodynamic force reads

$$\boldsymbol{F} = \frac{M_S}{RT\rho_S}\nabla\left(\mathrm{tr}\boldsymbol{\Sigma}\right). \tag{16.6}$$

The Eshelby energy-momentum tensor $\boldsymbol{\Sigma}$ depends on the stress-strain state of the host material. A material particle of micropolar continuum represents an infinitesimal rigid body. Its kinematic is described by independent displacement vector $\boldsymbol{u}$ and microrotation vector $\boldsymbol{\theta}$. Two strain measures, stretch tensor $\boldsymbol{\varepsilon}$ and wryness tensor $\boldsymbol{\kappa}$ can be expressed in terms of displacements and microrotations as follows [20]:

$$\boldsymbol{\varepsilon} = \nabla\boldsymbol{u} + \boldsymbol{I}\times\boldsymbol{\theta}, \qquad \boldsymbol{\kappa} = \nabla\boldsymbol{\theta}. \tag{16.7}$$

where $\boldsymbol{I}$ is the unit second-order tensor, operation $\times$ denotes vector product. Vector product of second-order tensor $\boldsymbol{A} = \boldsymbol{a}_k\boldsymbol{b}_k$ and vector $\boldsymbol{c}$ is given by $\boldsymbol{A}\times\boldsymbol{c} = \boldsymbol{a}_k\left(\boldsymbol{b}_k\times\boldsymbol{c}\right)$, hereafter the Einstein rule of summation over the repeated index is used.

The total strain tensors can be decomposed into elastic parts and eigenstrains due to accumulation of impurity, i.e. strains that would exist in material in the absence of constraint. Accumulation of gas is usually assumed to lead to dilatation only, so the total wryness tensor coincides with the elastic one given by the second equation (16.7), whereas the stretch tensor represents a sum of elastic stretch tensor $\boldsymbol{\varepsilon}^{el}$ and eigenstrains $\boldsymbol{\varepsilon}^* = \alpha c\boldsymbol{I}$ (α is the linear expansion coefficient) that is

$$\boldsymbol{\varepsilon} = \boldsymbol{\varepsilon}^{el} + \boldsymbol{\varepsilon}^*. \tag{16.8}$$

The strain energy density can be written as [26]

$$W = \frac{1}{2}\boldsymbol{\varepsilon}^{el}\cdot\cdot{}^4\boldsymbol{C}\cdot\cdot\boldsymbol{\varepsilon}^{el} + \boldsymbol{\varepsilon}^{el}\cdot\cdot{}^4\boldsymbol{B}\cdot\cdot\boldsymbol{\kappa} + \frac{1}{2}\boldsymbol{\kappa}\cdot\cdot{}^4\boldsymbol{D}\cdot\cdot\boldsymbol{\kappa}, \tag{16.9}$$

where ${}^4\boldsymbol{C}$, ${}^4\boldsymbol{B}$, ${}^4\boldsymbol{D}$ are tensors of elastic moduli.

The constitutive relations for the stress tensor $\boldsymbol{T}$ and couple stress tensor $\boldsymbol{M}$ read

$$\boldsymbol{T} = \frac{\partial W}{\partial \boldsymbol{\varepsilon}^{el}} = {}^4\boldsymbol{C} : \boldsymbol{\varepsilon}^{el} + {}^4\boldsymbol{B} : \boldsymbol{\kappa}, \qquad \boldsymbol{M} = \frac{\partial W}{\partial \boldsymbol{\kappa}} = {}^4\boldsymbol{B} : \boldsymbol{\varepsilon}^{el} + {}^4\boldsymbol{D} : \boldsymbol{\kappa}. \tag{16.10}$$

For an isotropic material ${}^4\boldsymbol{B} = 0$, and tensors of elastic moduli ${}^4\boldsymbol{C}$, ${}^4\boldsymbol{D}$ can be represented as linear combinations of isotropic fourth-order tensors ${}^4\boldsymbol{I}_1 = \boldsymbol{II}$, ${}^4\boldsymbol{I}_2 = \boldsymbol{e}_k\boldsymbol{I}\boldsymbol{e}_k$ and ${}^4\boldsymbol{I}_3 = \boldsymbol{e}_k\boldsymbol{e}_m\boldsymbol{e}_k\boldsymbol{e}_m$ as

$$\begin{aligned} {}^4\boldsymbol{C} &= \lambda {}^4\boldsymbol{I}_1 + 2G {}^4\boldsymbol{E} + \frac{\kappa}{2}\left({}^4\boldsymbol{I}_3 - {}^4\boldsymbol{I}_2\right), \\ {}^4\boldsymbol{D} &= \beta_1^4\boldsymbol{I}_1 + (\beta_2+\beta_3)\,{}^4\boldsymbol{E} + \frac{\beta_3-\beta_2}{2}\left({}^4\boldsymbol{I}_3 - {}^4\boldsymbol{I}_2\right), \end{aligned} \tag{16.11}$$

where ${}^4\boldsymbol{E} = 1/2\left({}^4\boldsymbol{I}_2 + {}^4\boldsymbol{I}_3\right)$, and λ, G are Lamé coefficients, $\kappa, \beta_1, \beta_2, \beta_3$ are micropolar elastic moduli.

The micropolar elastic moduli can be expressed in terms of engineering constants, namely, coupling number N, polar ratio ψ, characteristic length for torsion l_t and characteristic length for bending l_b in accordance with [27, 28] as follows

$$N = \sqrt{\frac{\kappa}{2G+\kappa}}, \quad N \in [0,1], \qquad \psi = \frac{\beta_2+\beta_3}{\beta_1+\beta_2+\beta_3}, \quad \psi \in [0,1.5], \tag{16.12}$$

$$l_t = \sqrt{\frac{\beta_2+\beta_3}{2G}}, \qquad l_b = \sqrt{\frac{\beta_3}{4G}}.$$

The steady-state of material is determined by the balances of linear and angular momentum that in the absence of body forces and couples are as follows:

$$\int_S \boldsymbol{n}\cdot\boldsymbol{T}\,\mathrm{dS} = \boldsymbol{0}, \qquad \int_S \left(\boldsymbol{n}\cdot\boldsymbol{M} + \boldsymbol{r}\times(\boldsymbol{n}\cdot\boldsymbol{T})\right)\mathrm{dS} = \boldsymbol{0}, \tag{16.13}$$

where $\boldsymbol{r}$ is the position vector of a material particle.

Equations (16.13) in local form reduce to

$$\nabla\cdot\boldsymbol{T} = \boldsymbol{0}, \qquad \nabla\cdot\boldsymbol{M} + \boldsymbol{T}_\times = \boldsymbol{0}, \tag{16.14}$$

where $\boldsymbol{A}_\times = (\boldsymbol{a}_k\boldsymbol{b}_k)_\times = \boldsymbol{a}_k\times\boldsymbol{b}_k$ is the vectorial invariant. Its invariant representation is given by $\boldsymbol{A}_\times = -\boldsymbol{A}\times\cdot\boldsymbol{I}$, where the mixed product of two second-order tensors is introduced as $\boldsymbol{A}\times\cdot\boldsymbol{B} = \boldsymbol{a}_k\boldsymbol{b}_k\times\cdot\boldsymbol{c}_m\boldsymbol{d}_m = (\boldsymbol{b}_k\times\boldsymbol{c}_m)\,(\boldsymbol{a}_k\cdot\boldsymbol{d}_m)$.

Within the micropolar linear elasticity, the Eshelby energy-momentum tensor appearing in Eq. (16.5) is defined as [23]

$$\boldsymbol{\Sigma} = W\boldsymbol{I} - (\nabla\boldsymbol{u} - \boldsymbol{\varepsilon}^*)\cdot\boldsymbol{T}^T - \nabla\boldsymbol{\theta}\cdot\boldsymbol{M}^T, \tag{16.15}$$

where the upper index T denotes a transposed second-order tensor ($\boldsymbol{A}^T = (\boldsymbol{a}_k\boldsymbol{b}_k)^T = \boldsymbol{b}_k\boldsymbol{a}_k$).

Substituting Eqs. (16.15), $(16.7)_1$–(16.10) in Eq. (16.6) and considering isotropic material, we obtain the following expression for the additional thermodynamic driving force:

$$\boldsymbol{F} = \frac{M_S}{RT\rho_S}\nabla\left(\frac{1}{2}(\nabla\boldsymbol{u} - \alpha c\boldsymbol{I})\cdot\cdot{}^4\boldsymbol{C}\cdot\cdot(\nabla\boldsymbol{u} - \alpha c\boldsymbol{I}) + \right. \tag{16.16}$$

$$\left. +2(\nabla\boldsymbol{u} - \alpha c\boldsymbol{I})\cdot\cdot{}^4\boldsymbol{C}\cdot\cdot(\boldsymbol{I}\times\boldsymbol{\theta}) + \frac{3}{2}(\boldsymbol{I}\times\boldsymbol{\theta})\cdot\cdot{}^4\boldsymbol{C}\cdot\cdot(\boldsymbol{I}\times\boldsymbol{\theta}) + \frac{1}{2}\nabla\boldsymbol{\theta}\cdot\cdot{}^4\boldsymbol{D}\cdot\cdot\nabla\boldsymbol{\theta}\right).$$

The last three terms in Eq. (16.16) appear due to the presence of independent microrotations of material particles and couple stress interactions between them. Their presence increases the value of the thermodynamic driving force. These terms vanish within the framework of the classical elasticity accounting for only translation degrees of freedom of material particles. The value of displacement's gradient, in turn, depends on stress-strain state caused by both accumulation of impurity and couple stress interactions between material particles. As a result, accounting for couple stress interactions between material particles results in increasing the first term in Eq. (16.16). So that, modeling of material particles by means of infinitesimal rigid bodies results in increasing the thermodynamic driving force. The question arises on the influence of such an increase on diffusion process.

The paper focuses on description of skin effects, so that in the following we seek for solution of initial boundary-value problem.

16.3 Axially Symmetric Problem

We restrict ourselves to consideration of an axially symmetric problem and model non-stationary stress-induced diffusion in a long cylinder of radius r_0. Cylindrical coordinate system (r, φ, z), where r, z denote respectively radial and axial coordinates and φ denotes azimuthal angle, is introduced, $\boldsymbol{e}_r$, $\boldsymbol{e}_\varphi$, $\boldsymbol{e}_z$ denote the basic vectors. Initial concentration inside cylinder is assumed to be zero.

To demonstrate the specificity of the influence of the additional thermodynamic driving force introduced in the previous section on the concentration profile regardless of the boundary conditions (BCs), we consider three possible types of BC on the lateral surface of the cylinder. In the first case a constant concentration is prescribed, that is

$$c|_{r=r_0} = c_0. \tag{16.17}$$

In the second case the diffusion flux is prescribed, i.e

$$D\frac{\partial c}{\partial r}\bigg|_{r=r_0} = J_0. \tag{16.18}$$

In the third case the diffusion flux is supposed to be proportional to the concentration difference, so

$$D\frac{\partial c}{\partial r}\bigg|_{r=r_0} = k\,(c - c_0)\,, \tag{16.19}$$

where k is the surface mass transfer coefficient, c_0 is a constant concentration maintained in a working chamber.

The lateral surface of the cylinder is supposed to be traction free, whereas a non-classical static boundary condition is used, so that

$$\boldsymbol{e}_r \cdot \boldsymbol{T}|_{r=r_0} = \boldsymbol{0}, \tag{16.20}$$

$$\boldsymbol{e}_r \cdot \boldsymbol{M}|_{r=r_0} = M_0 \boldsymbol{e}_\varphi. \tag{16.21}$$

Note that setting of microrotations on the border instead of external couples does not affect the solution qualitatively, see [29] for details.

The cylinder is not loaded axially, hence

$$\int_S \boldsymbol{e}_z \cdot \boldsymbol{T}\mathrm{dS}\bigg|_{z=0,z=L} = \boldsymbol{0}, \qquad \int_S \boldsymbol{e}_z \cdot \boldsymbol{M}\mathrm{dS}\bigg|_{z=0,z=L} = \boldsymbol{0}, \tag{16.22}$$

where L is the length of the cylinder.

Assuming all cross-sections behave similarly, we seek a solution with the following ansatz:

$$c = c\,(r)\,, \tag{16.23}$$

$$\boldsymbol{u} = u_r\,(r)\,\boldsymbol{e}_r + U_z\,(r,z)\,\boldsymbol{e}_z, \tag{16.24}$$

$$\varepsilon_{zz} = \frac{\partial U_z}{\partial z} = \mathrm{const}, \tag{16.25}$$

$$\boldsymbol{\theta} = \theta_r\,(r)\,\boldsymbol{e}_r + \theta_z\,(r)\,\boldsymbol{e}_z. \tag{16.26}$$

From Eq. (16.25) it follows that

$$U_z\,(r,z) = u_z\,(r) + \widetilde{u}_z\,(z)\,. \tag{16.27}$$

At the center of the cylinder the following boundary conditions are prescribed:

$$\frac{\partial c}{\partial r}\bigg|_{r=0} = 0, \tag{16.28}$$

$$u_r|_{r=0} < \infty, \qquad u_z|_{r=0} = 0, \qquad \theta_r|_{r=0} = \theta_\varphi\big|_{r=0} = 0. \tag{16.29}$$

System of equations for concentration c, axial stretch strains $\varepsilon_{zz} = \partial U_z/\partial z$, radial displacement u_r, axial displacement u_z and microrotation θ_φ takes form

$$r\dot{c} = [rD\,(c' + cF)]', \quad \text{where} \tag{16.30}$$

$$F = \frac{M_S}{RT\rho_S}\left[\frac{\lambda}{2}\left(\varepsilon_{zz} + u_r' + \frac{u_r}{r}\right)^2 + G\left(\left(\frac{u_r}{r}\right)^2 + (u_r')^2 + (\varepsilon_{zz})^2\right) - \right. \tag{16.31}$$

$$\left. -2\,(3\lambda + 2G)\,\alpha\left(\varepsilon_{zz} + u_r' + \frac{u_r}{r}\right)c + \frac{9}{2}\,(3\lambda + 2G)\,\alpha^2 c^2 + \right.$$

$$+G\left(\frac{3}{2N^2}\left(u_z'\right)^2+2l_b^2\left[\left(\theta_\varphi'\right)^2+\left(\frac{\theta_\varphi}{r}\right)^2\right]-2\left(l_t^2-2l_b^2\right)\frac{\theta_\varphi}{r}\theta_\varphi'\right)\Bigg]',$$

$$\int_0^{r_0}\left[(\lambda+2G)\,\varepsilon_{zz}+\lambda\left(u_r{}'+\frac{u_r}{r}\right)-(3\lambda+2G)\,\alpha c\right]rdr=0, \tag{16.32}$$

$$\left(ru_r'\right)'-\frac{u_r}{r}-\frac{(3\lambda+2G)}{(\lambda+2G)}\alpha\left((rc)'-c\right)=0, \tag{16.33}$$

$$\left(ru_z{}'\right)'+2N^2\left(r\theta_\varphi\right)'=0, \tag{16.34}$$

$$2l_b^2\left(r\theta_\varphi'\right)'-\left(\frac{2}{r}l_b^2+r\frac{2N^2}{1-N^2}\right)\theta_\varphi-r\frac{N^2}{1-N^2}u_z{}'=0, \tag{16.35}$$

where $\dot{c}$ is the partial derivative of concentration with respect to time, $'$ denotes derivation with respect to radial coordinate. Note that equation for θ_r has a trivial solution and is not provided.

Let us analyze the expression for the additional thermodynamic driving force F given by Eq. (16.31). In fact, it consists of two parts. The first part depends on the solution of the elasticity problem due to the mass transport, whereas the second one depends on the solution of the micropolar boundary-value problem. Solutions of these two problems are independent, since Eqs. (16.34)–(16.35) can be solved independently on the general system of equations and provide behavior of a non-saturated solid, which is not changed with time. In [29] we demonstrated that an approximate solution of the micropolar boundary-value problem can be found analytically. In accordance with [29], this solution decreases exponentially with distance from the border as

$$u_z\approx-\frac{M_0}{2G}\exp\left(-\frac{N}{l_b}\left(r_0-r\right)\right),\qquad \theta_\varphi\approx\frac{M_0}{4GNl_b}\exp\left(-\frac{N}{l_b}\left(r_0-r\right)\right). \tag{16.36}$$

The microrotation is a rapidly decreasing function, so that terms with $\theta_\varphi\theta_\varphi'/r$ and $\left(\theta_\varphi/r\right)^2$ in Eq. (16.31) can be neglected. Accounting for the couple stress interactions between material particles increases the value of the thermodynamic driving force in the vicinity of the border. The value of this driving force depends on the distributed couple stress M_0 and non-classical material parameters l_b, N. Increasing of M_0 results in increasing the absolute values of F, but does not change significantly the area of function's decay, which is mainly determined by the ratio N/l_b. Increasing of the value N/l_b, in turn, results both in increasing the absolute value of the thermodynamic driving force and in decreasing the area of function's decay. As a result, an increase of the ratio of the coupling number and characteristic length for bending leads to a more dramatic change in the concentration profile in comparison with the result obtained under consideration of a smaller value. Such a change can be caused both by increasing the coupling number and by decreasing the characteristic length for bending. At the same time, decreasing of l_b plays a more significant role, since in fact F is determined by terms proportional to $N\exp\left(-N\left(r_0-r\right)/l_b\right)/l_b^3$.

We seek for numerical solution of the partially coupled diffusion-elasticity problem. To this end, a numerical scheme is developed. The main specificity of the scheme is discussed in the Appendix. In [29] we demonstrated that an approximate analytical solution to the micropolar boundary-value problem is in good agreement with the corresponding numerical solution, so that the above discussion on behavior of the additional thermodynamic driving force must be true for both for analytical and numerical solutions.

16.4 Results and Discussion

We investigate the specificity of the developed model by an example of diffusion of hydrogen in a standard cylindrical steel specimen of radius 4 mm and length 40 mm. Experiment on the hydrogen saturation of such a specimen and the subsequent estimation of the inner concentration were carried out in [5, 30]. The tested specimen was incubated at room temperature for 96 hours in a deaerated solution based on distilled water with 5 wt% NaCl and 0.5 wt% CH_3COOH. The gaseous hydrogen sulfide was purged through the solution by bubbling. A constant concentration of 2500 mg/l of hydrogen sulfide was maintained in the working chamber.

Material parameters of steel and characteristics of impurity are given in Table 16.1, see [24] for details. We consider three values of the distributed couple stress, namely, $M_0 = -150\,\mathrm{kPa}\cdot\mathrm{m}$, $M_0 = -100\,\mathrm{kPa}\cdot\mathrm{m}$ and $M_0 = -50\,\mathrm{kPa}\cdot\mathrm{m}$.

We first assume that a constant concentration c_0 is prescribed on the border. According to [5], 2500 mg/l of hydrogen sulfide maintained on the boundary corresponds to concentration of about 50 ppm w.r.t. mass. Figure 16.1 compares the results obtained under consideration classical Fick's law ($\mu_S = 0$), nonlocal Fick's

Table 16.1: Material parameters of steel and characteristics of impurity.

Parameter	Value
Steel	
Molar mass, M_S	$0.056\,\mathrm{kg/mol}$
Density, ρ_S	$7800\,\mathrm{kg/m^3}$
Lamé coefficients, λ and G	120 GPa and 80 GPa
Characteristic length for bending, l_b	$7\,\mu$m, $10\,\mu$m, $13\,\mu$m
Coupling number, N	0.7, 0.9
Impurity	
Molar mass, M_H	$0.002\,\mathrm{kg/mol}$
Linear expansion coefficient, α	$1.5\cdot 10^{-6}$
Diffusion coefficient, D	$5\cdot 10^{-16}\,\mathrm{m^2/s}$

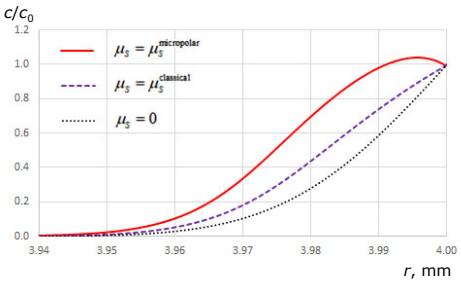

Fig. 16.1 Concentration profiles obtained at different constitutive equations for the diffusion flux

law accounting for the chemical potential of solid host material calculated within the classical elasticity ($\mu_S = \mu_S^{\text{classical}}$) and nonlocal Fick's law accounting for the chemical potential of solid host material calculated within the micropolar elasticity ($\mu_S = \mu_S^{\text{micropolar}}$ at $l_b = 13\,\mu$m, $N = 0.9$, $M_0 = -100\,\text{kPa}\cdot\text{m}$). It is seen that in the case of nonlocal diffusion laws the impurity tends to accumulate in the vicinity of the border more intensive than in the case of local law. Accounting for the couple stress interactions between material particles results in the largest local increase in hydrogen concentration. The main specificity of the model with $\mu_S = \mu_S^{\text{micropolar}}$ is that starting at some point in time concentration in the vicinity of the border becomes bigger than the one prescribed on the border ($c/c_0 > 1$).

As discussed in Sect. 16.2, the expression of the diffusion flux in terms of a sum of chemical potentials of components of the system "impurity-host material" results in consideration of thermodynamic driving forces of different nature. The first one is due to the concentration difference, whereas the second one is due to the stress-strain state of the host material. Obviously, these forces can be unidirectional or multidirectional. The chemical potential of solid matrix, in turn, depends on the stress-strain state caused both by the self-stresses due to accumulation of hydrogen and by the presence of the distributed couples on the lateral surface. Accumulation of impurity results in increasing the chemical potential within the hydrogenated area, and accounting for the couple stress interactions results in increasing the chemical potential in the vicinity of the border. So that, the chemical potential of solid takes its maximum directly on the border and rapidly decreases with distance. As a result, diffusion flux due to the gradient of the chemical potential of solid host material is always directed from the outer areas into the inner areas of material.

Figure 16.2 presents concentration profiles at different time of saturation the metal specimen with hydrogen. Solution of the problem obtained within the micropolar approach is considered. One can see a fast accumulation of impurity near the border, which does not have time to diffuse into deeper areas of the material before a new portion of impurity comes. Moreover, despite we consider an open system and take into account that impurity in principle can be extracted from the cylinder, the resulting diffusion flux is directed from the border inside cylinder, but not from the cylinder to the working chamber even after concentration exceeds the one prescribed on the surface. So that, presence of couple stress interactions in material can be considered as a reason of the appearance of a source term in the diffusion equation.

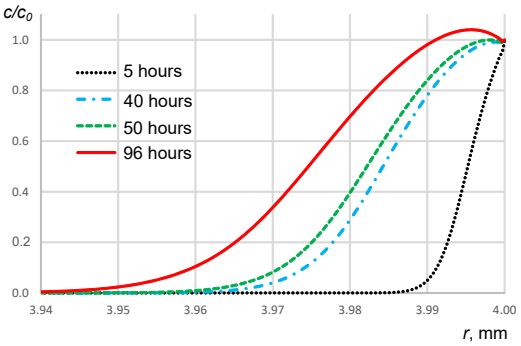

Fig. 16.2 Concentration profiles at different time of saturation with hydrogen

Figure 16.3 shows the influence of non-classical material parameters on the concentration profiles after 96 hours of saturation with hydrogen. It is seen that as discussed in the previous section, increasing of the coupling number and decreasing of the material length for bending results in a more dramatic change of the concentration profile in the vicinity of the border.

Figure 16.4 compares the concentration profiles at two values of the distributed couple stress on the lateral surface at $l_b = 13\,\mu$m, $N = 0.9$. Increasing of M_0 also results in a more dramatic change of the concentration profile in the vicinity of the border.

Instead of the Dirichlet BC given by Eq. (16.17) one can use the Robin BC given by Eq. (16.19) at an infinite surface mass transfer coefficient ($k \to \infty$). In this case concentration on the border tends to instantly take on value c_0 maintained in a working chamber. However, real diffusion processes have a finite velocity, so that $k < \infty$ and $c|_{r=r_0} - c_0 \neq 0$. Figure 16.5 presents the concentration profiles at two values of k at different time ($l_b = 13\,\mu$m, $N = 0.9$, $M_0 = -100\,\text{kPa}\cdot\text{m}$). Again it is seen that impurity accumulates rapidly in the vicinity of the border resulting in an excess of hydrogen. Decreasing of the mass transfer coefficients results in smaller values of concentration, but does not change the result qualitatively.

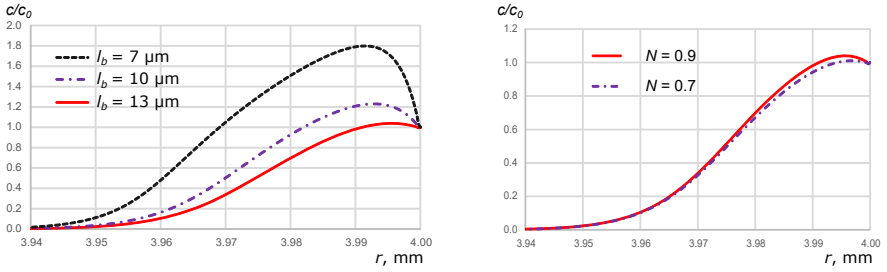

Fig. 16.3: Concentration profiles after 96 hours of saturation with hydrogen at fixed $N = 0.9$ (left) and fixed $l_b = 13\,\mu$m (right).

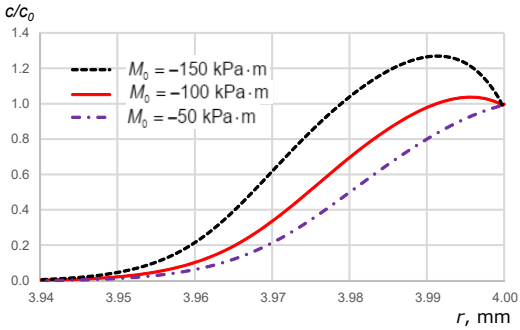

Fig. 16.4 Concentration profiles after 96 hours of saturation with hydrogen at different values of the distributed couple stress on the lateral surface

Let us finally prescribe a constant nonzero flux in a working chamber that can be described by the Neumann BC given by Eq. (16.18), $J_0 = 5 \cdot 10^{-10}$ m/s. Comparison of the results presented at Figs. 16.2–16.6 allows to conclude that the presence of a "hump" on the concentration profile is a general specificity of the model of stress-induced diffusion accounting for the chemical potential calculated within the micropolar theory. The presence of a relatively large distributed couple stress on the border results in a significantly non-uniform stress-strain state of material and leads to a local increase of concentration in the vicinity of the outer surface. In principle, such a dramatic change in chemical potential of the solid could be observed even in the case of modeling the host material by classical continuum. However, the appearance of such a big eigenstrains seems to be non-physical. At the same time, couple stress interactions between material particles indeed may play a significant role in the vicinity of the border. Note that values of M_0 used in the paper correspond to microrotation of surface elements less than a few degrees that correlates with physical concepts [31].

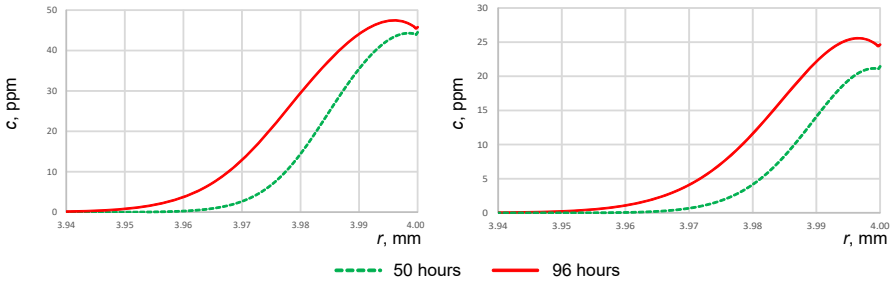

Fig. 16.5: Concentration profiles at different time of saturation with hydrogen in the case of the Robin BC on the lateral surface of the cylinder: $k = 5 \cdot 10^{-10}$ m/s (left) and $k = 5 \cdot 10^{-11}$ m/s (right).

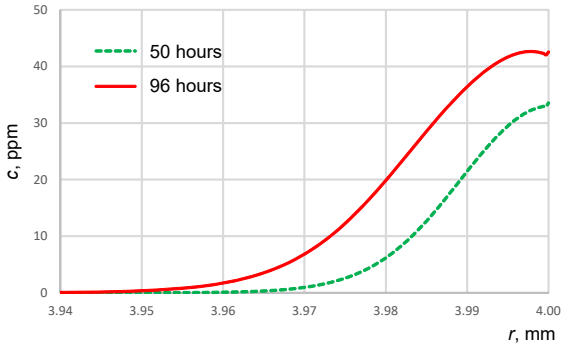

Fig. 16.6 Concentration profiles at different time of saturation with hydrogen in the case of the Neumann BC on the lateral surface of the cylinder

16.5 Conclusions

The paper proposed a model of stress-induced diffusion due to the gradient of chemical potential of solid host material modeled by means of the microstructure-informed micropolar continuum. The model is a generalization of the corresponding model developed in literature within classical theory. Consideration of general expression for the Eshelby energy-momentum tensor allows one to account for couple stress interaction between material particles that plays a role in the vicinity of the area of disturbance. As a result, the model can be implemented to describe size effects due to the presence of inhomogeneities. The paper focused on investigation of skin effect that is an excess of concentration in the vicinity of the saturated border. It was shown that application of nonlocal Fick's law results in a fast saturation of the boundary layer of material. In the case of relatively big values of couple stresses fluxes caused by the concentration gradient and by the solid's chemical potential gradient become multi-directional at some time instant. As a result, the concentration in the vicinity of the border may exceed on the border. Such a situation leads to a significant local increase of impurity concentration, which can worsen material properties and even lead to its damage and so that must be taken into account.

Appendix: Some Remarks on Numerical Approximation

Numerical methods can be both conservative and non-conservative that means they ensure conservation of physical characteristics that are mass, linear and angular momentum, or do not [32]. Within the research we tried our best to follow the principle of "conservativity". In the following we briefly provide the main stages of our numerical approximation.

To obtain a conservative numerical approximation, it is preferred to deal with integral equations describing the physical laws, but not with differential equations providing corresponding local balances. So that it is preferred to deal with mass balance given by Eq. (16.1), and balances of linear and angular momentum given

by Eqs. (16.13).Solution of the system of integral equations in the given form is a challenging task due to the complexity of solving Eq. (16.13). To overcome the problem, we simplify the second equation (16.13) through accounting for the balance of linear momentum given by first equation. So that, instead of numerical approximation of the term "$-\nabla\cdot(\boldsymbol{T}\times\boldsymbol{r})$" appearing after replacement of surface integral by volume integral we approximate the term "$-\boldsymbol{T}\times\cdot\nabla\boldsymbol{r}=-\boldsymbol{T}\times\cdot\boldsymbol{I}=\boldsymbol{T}_{\times}$", which can be obtained taking into account that after parenthesis expansion the term "$-(\nabla\cdot\boldsymbol{T})\times\boldsymbol{r}$" vanishes. Note that it is a usual practice when passing from the integral form of the balance of angular momentum to the local form. As a result, we deal with the modified system of integral equations

$$\int_V \dot{c}\,\mathrm{dV}=-\int_{\mathrm{V}}\nabla\cdot\boldsymbol{J}\,\mathrm{dV},\quad \int_{\mathrm{V}}\nabla\cdot\boldsymbol{T}\,\mathrm{dV}=\boldsymbol{0},\quad \int_{\mathrm{V}}(\nabla\cdot\boldsymbol{M}+\boldsymbol{T}_{\times})\,\mathrm{dV}=\boldsymbol{0}.$$

In fact, Eqs. (16.1), the first equation of (16.13) remain unchanged, and the second one is modified. This makes the form of integral equation corresponding to balance of angular momentum to be non-conservative, whereas forms of the mass balance and balance of linear momentum are conservative.

Numerical approximation of divergence of tensor function $\boldsymbol{\Phi}$ is also made on the base of a known definition in terms of integrals written for an elementary domain V surrounded by surface S:

$$\nabla\cdot\boldsymbol{\Phi}=\lim_{V\to 0}\frac{\int_S \boldsymbol{n}\cdot\boldsymbol{\Phi}\,\mathrm{dS}}{V}.$$

In the case of cylindrical coordinate system divergence of an arbitrary tensor function $\boldsymbol{\Phi}$ is defined as

$$\nabla\cdot\boldsymbol{\Phi}=\frac{1}{r}\boldsymbol{e}_r\cdot\frac{\partial}{\partial r}(r\boldsymbol{\Phi})+\frac{1}{r}\frac{\partial}{\partial\varphi}(\boldsymbol{e}_{\varphi}\cdot\boldsymbol{\Phi})+\boldsymbol{e}_z\cdot\frac{\partial\boldsymbol{\Phi}}{\partial z}. \tag{16.37}$$

Note that application of Eq. (16.37) without removing the brackets makes a sense only in the case of numerical solution to obtain a conservative approximation. In the case of analytical solution, brackets can be removed as usually done.

Solution of the problem considered in the paper depends only on the radial coordinate. So that, a one-dimensional mesh is introduced to obtain a numerical solution. Concentration, displacements and microrotations are specified in mesh nodes, whereas fluxes, deformations and stresses are specified in mesh cells. Differential equations (16.30)–(16.35) were obtained under application of Eq. (16.37) written for ∇-operator in cylindrical coordinates. These equations are further approximated by finite differences to define the stress–strain state in the inner nodes and cells. Solution in the end nodes, in turn, can be found both by "fixing" boundary conditions or "naturally" from integral conversation laws. The first way is used when kinematic boundary conditions are specified within elastic problem (Eqs. (16.17), (16.29)) and when concentration is prescribed on the border (Eq. (16.17)). The second way is used when static boundary conditions are prescribed within the the framework of

elasticity problem (Eq. (16.20), (16.21)) and when diffusion fluxes are given within diffusivity problem (Eqs. (16.18), (16.19), (16.28)).

References

[1] Koyama M, Akiyama E, Lee Y-K, Raabe D, Tsuzaki K (2017) Overview of hydrogen embrittlement in high-Mn steels, Int J Hydrog Energy **42**(17):12706-12723.
[2] Wasim M, Djukic MB (2020) Hydrogen embrittlement of low carbon structural steel at macro-, micro-and nano-levels, Int J Hydrogen Energy **45**(3):2145-2156.
[3] Wu TI, Wu JC (2008) Effects of cathodic charging and subsequent solution treating parameters on the hydrogen redistribution and surface hardening of Ti–6Al–4V alloy, J Alloys Compd **466**(1-2):153-159.
[4] Martinsson Å, Sandström R (2012) Hydrogen depth profile in phosphorus-doped, oxygen-free copper after cathodic charging, J Mater Sci **47**(19):6768-6776.
[5] Polyanskiy VA, Belyaev AK, Alekseeva EL, Polyanskiy AM, Tretyakov DA, Yakovlev YA (2019) Phenomenon of skin effect in metals due to hydrogen absorption, Continuum Mech Thermodyn **31**(6):1961-1975.
[6] Aifantis EC (1980) On the problem of diffusion in solids, Acta Mech **37**(3):265-296.
[7] Indeitsev D, Mochalova Y (2014) Mechanics of multi-component media with exchange of mass and non-classical supplies, In: Irschik H, Belyaev AK (Eds) Dynamics of Mechanical Systems with Variable Mass, pp 165-194, Springer, Vienna.
[8] Indeitsev DA, Mochalova YA (2017) On the problem of diffusion in materials under vibrations, In: Altenbach H, Goldstein R, Murashkin E (Eds) Mechanics for Materials and Technologies, pp 183-193, Springer, Cham.
[9] Belyaev AK, Polyanskiy VA, Yakovlev YA (2012) Stresses in a pipeline affected by hydrogen, Acta Mech **223**(8):1611-1619.
[10] Wu CH (2001) The role of Eshelby stress in composition-generated and stress-assisted diffusion, J Mech Phys Solids **49**(8):1771-1794
[11] Li JCM, Oriani RA, Darken LS (1966) The thermodynamics of stressed solids, Z Phys Chem **49**(3-5):271-290.
[12] Larché F, Cahn JW (1973) A linear theory of thermochemical equilibrium of solids under stress, Acta Metall **21**(8):1051-1063.
[13] Larchté, F.C., Cahn, J.L.: The effect of self-stress on diffusion in solids. Acta Metall. **30**(10), 1835–1845 (1982)
[14] Eshelby JD (1975) The elastic energy–momentum tensor, J Elast **5**(3-4):321-335.
[15] Mindlin RD (1965) Second gradient of strain and surface-tension in linear elasticity, Int J Solids Struct **1**(4):417-438.

[16] Mindlin RD, Eshel NN: On first strain-gradient theories in linear elasticity, Int J Solids Struct **4**(1):109-124.
[17] Toupin R (196(2) Elastic materials with couple-stresses, Arch Ration Mech Anal **11**(1):385-414.
[18] Aifantis EC (2003 Update on a class of gradient theories, Mech Mater **35**(3-6), 259-280.
[19] Altenbach, H., Eremeyev, VA (2012) Generalized Continua - from the Theory to Engineering Applications, Springer Science & Business Media.
[20] Eremeyev VA, Lebedev LP, Altenbach H (2012) Foundations of micropolar mechanics. Springer Science & Business Media (2012)
[21] Maugin GA, Metrikine AV (Eds): Mechanics of Generalized Continua, Springer, New York (2010)
[22] Eremeev VA, Zubov LM Phase-equilibrium conditions in nonlinear-elastic media with microstructurel Doklady Akad Nauk Minerologia USSR **322**(6):1052-1056.
[23] Lazar M, Kirchner HOK (2007) The Eshelby stress tensor, angular momentum tensor and scaling flux in micropolar elasticity, Int J Solids Struct **44**(14-15):4613-4620.
[24] Frolova KP, Vilchevskaya EN, Bessonov NM (2022) On modeling of stress-induced diffusion within micropolar and classical approaches, ZAMM - Z für Angew Math Mech **102**(6):e202100505 (2022)
[25] Cui Z, Gao F, Qu J (2012) A finite deformation stress-dependent chemical potential and its applications to lithium ion batteries, J Mech Phys Solids **60**(7):1280-1295.
[26] Nowacki W (1974) The linear theory of micropolar elasticity In: Nowacki W, Olszak W (Eeds) Micropolar Elasticity, International Centre for Mechanical Sciences, vol 151, pp 1-43, Springer, Vienna.
[27] Eringen AC (1999) Theory of micropolar elasticity. Microcontinuum field theories, Springer, New York, NY.
[28] Lakes R (2001) Elastic and viscoelastic behavior of chiral materials, Int J Mech Sci **43**(7):1579-1589.
[29] Frolova K, Vilchevskaya E, Bessonov N, Müller W, Polyanskiy V, Yakovlev Y (2022) Application of micropolar theory to the description of the skin effect due to hydrogen saturation, Math Mech Solids **27**(6):1092-1110.
[30] Alekseeva EL, Belyaev AK, Zegzhda AS, Polyanskiy AM, Polyanskiy VA, Frolova KP, Yakovlev YA (2018) Boundary layer influence on the distribution of hydrogen concentrations during hydrogen-induced cracking test of steels, Diagnostics, Resource and Mechanics of Materials and Structures **3**:43-57.
[31] Merson E, Kudrya AV, Trachenko VA, Merson D, Danilov V, Vinogradov A (2016) The Use of Confocal Laser Scanning Microscopy for the 3D Quantitative Characterization of Fracture Surfaces and Cleavage Facets, Procedia Struct Integr **2**:533-540.
[32] Samarskii AA (2001) The Theory of Difference Schemes, vol. 240, CRC Press, Boca Raton.